iScience

CellPress
OPEN ACCESS

Article

Ridge and crossrib height of butterfly wing scales is a toolbox for structural color diversity

Cédric Finet,[1,9,*] Qifeng Ruan,[2,3,*] Yi Yang Bei,[1,4] Vinodkumar Saranathan,[5,6,7,8] and Antónia Monteiro[1,*]
[1]Biological Sciences, National University of Singapore, Singapore 117543, Singapore
[2]Guangdong Provincial Key Laboratory of Semiconductor Optoelectronic Materials and Intelligent Photonic Systems, Harbin Institute of Technology, Shenzhen 518055, P.R. China
[3]Quantum Science Center of Guangdong-Hong Kong-Macao Greater Bay Area (Guangdong), Shenzhen 518045, P.R. China
[4]Max Planck Institute of Molecular Cell Biology and Genetics, Pfotenhauerstraße 108, 01307 Dresden, Germany
[5]Division of Science, Yale-NUS College, National University of Singapore, Singapore 138609, Singapore
[6]NUS Nanoscience and Nanotechnology Initiative (NUSNNI), National University of Singapore, Singapore 117581, Singapore
[7]Division of Sciences, School of Interwoven Arts and Sciences, Krea University, Sri City, Andhra Pradesh, India
[8]Present address: Institut de Recherche sur la Biologie de l'Insecte, UMR 7261, CNRS, Université de Tours, Tours, 37200 France
[9]Lead contact
*Correspondence: cedric.finet@ens-lyon.org (C.F.), ruanqifeng@hit.edu.cn (Q.R.), antonia.monteiro@nus.edu.sg (A.M.)
https://doi.org/10.1016/j.isci.2026.115374

SUMMARY

Butterfly wing vivid colors arise from light reflecting off cuticular scales, whose architecture consists of longitudinal ridges and transverse crossribs connected to a lower lamina by trabeculae. While the lower lamina's reflective properties are known in simpler scales, the upper surface's optical characteristics have only been thoroughly investigated in the case of modified ridges. This study examines how the lower lamina and the upper surface contribute to hue, brightness, and saturation across species. In *Bicyclus anynana*, ridge height changes correlate with hue shifts from artificial selection. This relationship holds true across 39 scale types in 34 species. By combining focused ion beam milling, microspectrophotometry, and optical modeling, we found that modifying ridge height is sufficient to change ridge hue, notably in *Morpho didius,* whose color was thought to be generated exclusively by ridge lamellae. This study identifies the upper surface of scales as a toolbox for structural color diversity in butterflies and proposes a geometrical model for predicting color that unifies species with and without Morpho-type ridges.

INTRODUCTION

Organismal structural colors result from the reflection of specific wavelengths of light by sub-micrometer structures found in biological materials.[1–3] In butterflies, structural colors originate primarily from the scales that cover the wing membrane.[4–6] These scales, around 100 μm in length, are the dead cuticular skeletons of single epidermal cells that grow and project out of the epithelial layer during pupal development. Scales are highly diverse in morphology,[7–10] but most share a common Bauplan with an upper surface made of a grid of longitudinal ridges and transverse crossribs defining open windows. Pillars, or trabeculae, support this grid structure on a lower lamina (LL) of finite thickness.[11] This Bauplan is believed to represent the scales found in the last common ancestor of extant butterflies.[12]

In these architecturally simple, stereotypical scales, structural color production is predominantly via light interacting with the LL that acts as a thin film reflector.[13,14] Variation in the thickness of this LL across nymphalid butterflies changes the color hue produced by thin-film interference.[14–17] Similar thin-film structural coloration has been described in scales formed of a fused upper and LL in extant butterflies[18,19] and primitive Lepidoptera.[20,21] In less frequent instances, ridges underwent morphological changes to become the primary reflectors,[8,22,23] sometimes in addition to the color produced by the LL.[24] This current view, however, is incomplete as it does not consider the contribution of the upper lamina to color generation in simple scales without exaggerated ridge modifications. Independently, a noteworthy recent study showed that engineered ridge-like nanostructures made of transparent chitosan (i.e., highly deacetylated chitin) produced the entire structural color palette via variations in height alone.[25] Because these vertical nanostructures are reminiscent of the butterfly scale ridges and crossribs, we explored if the height of these structures could explain their color. Here we demonstrate the important role of the height of this upper surface, specifically of the longitudinal ridges, in generating structural coloration even in stereotypical ''simple'' butterfly wing scales.

RESULTS

The upper surface substantially contributes to the overall scale coloration

To disentangle the relative contributions of upper surface and LL on scale coloration, we measured reflectance and compared

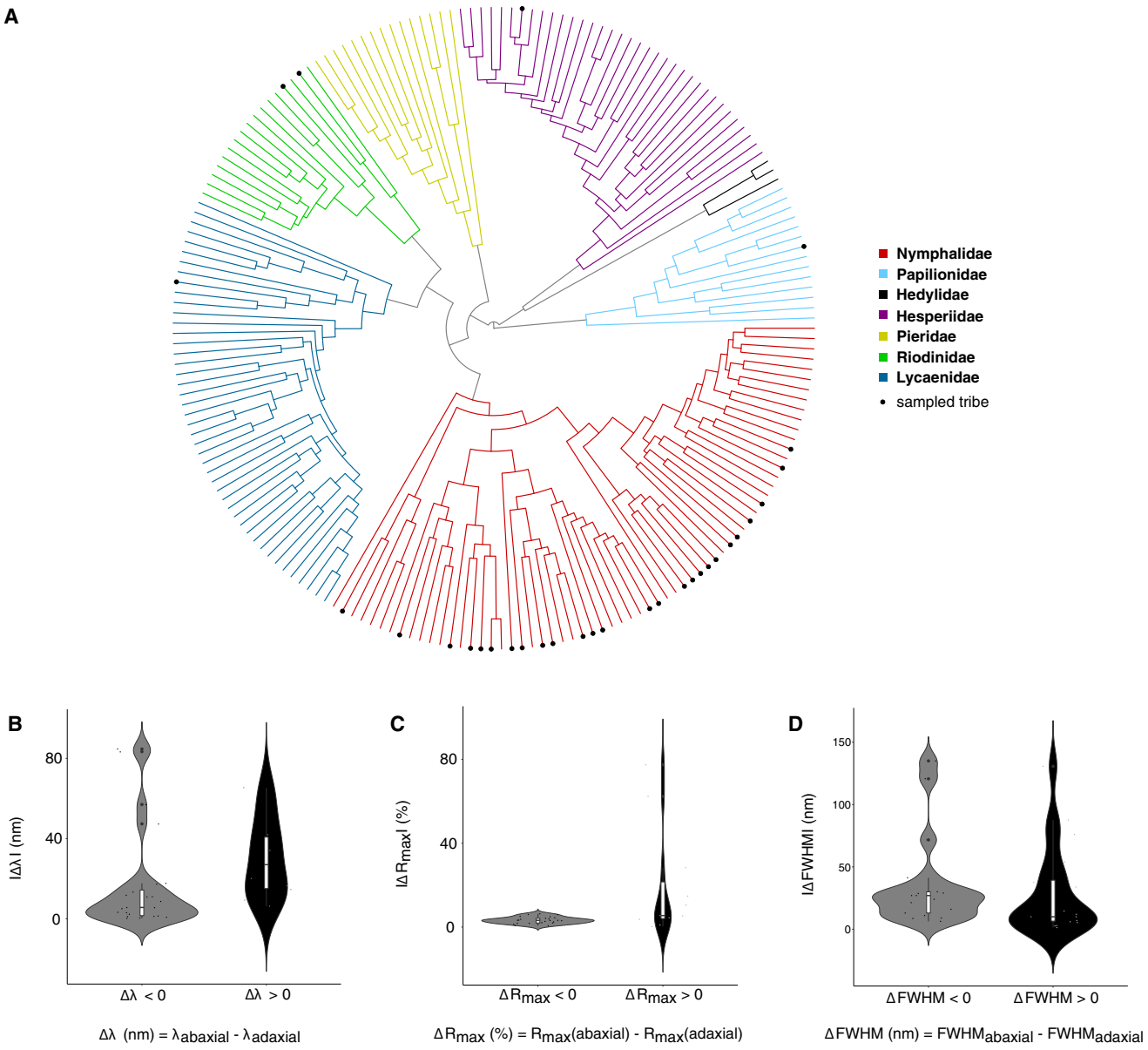

Figure 1. Contribution of the upper surface to the overall scale coloration

(A) Samples used in this study are mapped onto the phylogeny of butterflies by Espeland et al. 2018.[26]

(B–D) Distribution of the absolute value of shift in peak reflectance, reflectance intensity, and saturation, toward lower or higher wavelengths in the visible light spectrum. The central line in the violin plot indicates the median of the distribution, while the top and bottom of the box represent the third and first quartiles of the data, respectively. The whiskers show up to 1.5 times the inter-quartile range.

how light was reflected from the upperside (abwing side) and underside (adwing side) surfaces of 39 scales with stereotypical morphologies from 34 species (Figure 1A). This allowed us to quantify how much the upper surface modulates the thin-film structural color produced by the LL. We restricted our sampling to scales with the simple, "ancestor-like" Bauplan. Thus, we excluded broadband reflective scales that contain a contiguous upper lamina with no windows,[27–31] as well as scales having a modified lumen filled with multilayers or highly ordered photonic crystals.[11,32–35] Our dataset, however, included scales with *Morpho*-type ridges that have lamellae accentuated in size and number, but still display a stereotypical scale morphology.

We found that the upper surface nearly always shifted the reflectance peak, or hue, of the LL to either higher or lower wavelengths, depending on the sample, with the absolute shift in reflectance peak ranging from approximately 0 to 85 nm (Figures 1B and S1). The upper surface could also either increase or decrease the reflectance intensity of a scale (Figure 1C). In the

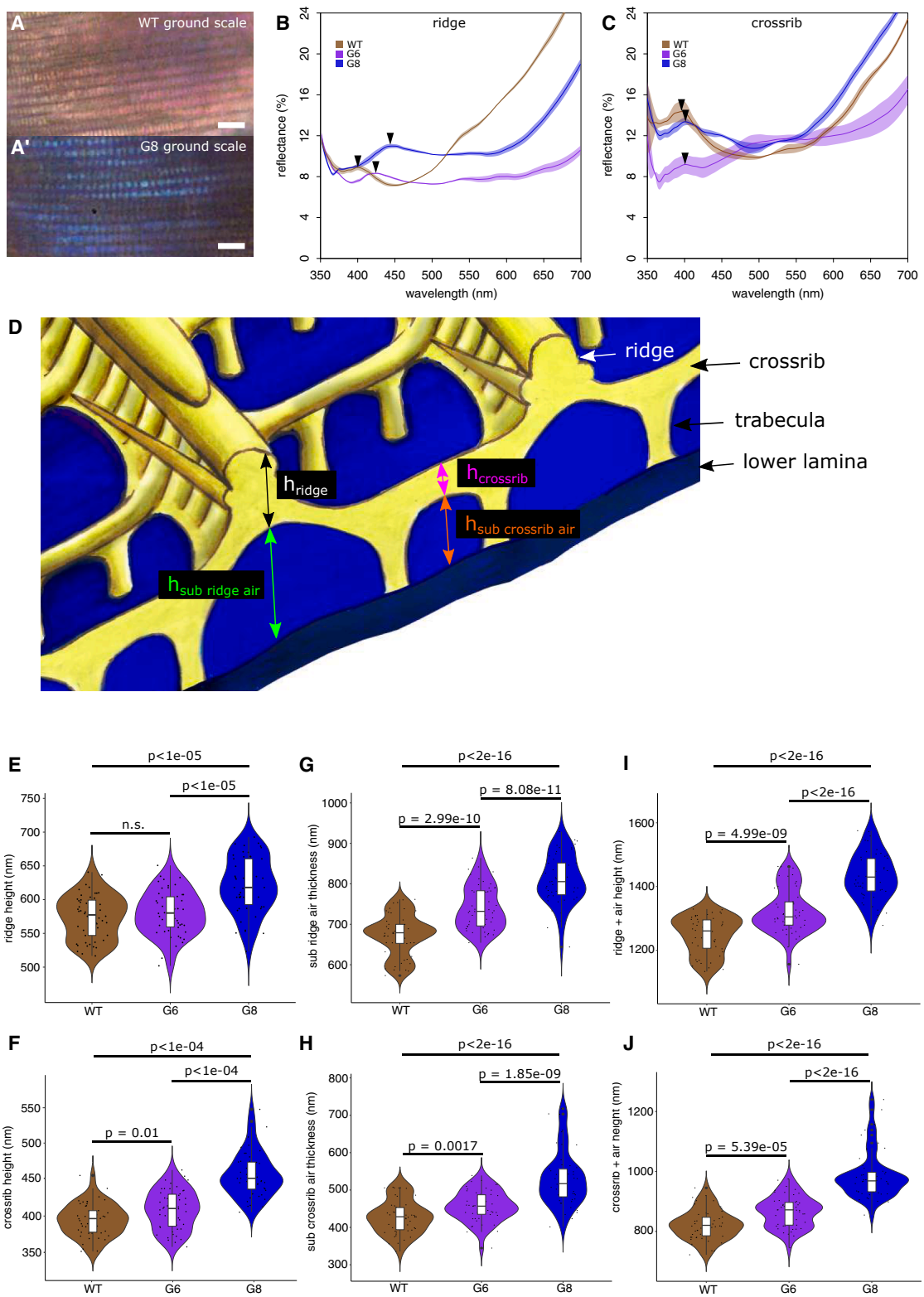

Figure 2. Evolution of scale reflectance and thicknesses of upper surface nanostructures over the course of an artificial selection experiment in *B. anynana* that targeted (blue) scale hue

(A and A′) Optical microscopy images of the abwing side of WT and violet-blue line (G8) ground scales. Scale bars are 4 μm.

(legend continued on next page)

majority of species, the upper surface decreased reflectance by a small amount, but in a small proportion of species, this surface contributed to a very large increase in reflectance intensity (Figure S1). For instance, the intensity of the blue ground scales in *Morpho sulkowskyi* increases by 77% through light reflecting from its upper surface nanostructures. Finally, we found that the upper surface can also either increase or decrease color "purity", or saturation, similarly in a bi-directional manner (Figures 1D and S1). The mapping onto the phylogenetic tree of the shift in peak reflectance, reflectance intensity, and saturation, between upper and lower surfaces, does not indicate a clear phylogenetic signal (Figure S1), i.e., the trait appears to be randomly distributed across the tips of the tree, rather than being clustered among related groups. This phylogenetic lability in the evolution of upper surface coloration is consistent with previous studies showing that scale structure can vary significantly among butterflies,[10] including intrageneric and intraspecific differences in the case of sexual dimorphism.[36–38] In summary, our reflectance measurements show that the upper surface—and its associated nanostructures—impacts the final hue and brightness of the scale in most of the scales investigated in this study.

Artificial selection acts on the geometry of the upper surface to evolve structural color

To further examine the contribution of the upper surface of scales in the generation of color, we revisited an artificial selection experiment performed on scale hue in *Bicyclus anynana* butterflies. This experiment produced violet-blue scales from UV-reflecting brown ground scales over eight generations of artificial selection in the laboratory.[15] The overall violet-blue coloration was shown to result, at least in part, from an increased thickness of the LL.[15] By re-examining conserved, dried specimens used to establish the violet-blue lines, we now further observed that the ridges and crossribs also acquired a violet-blue coloration (Figures 2A and 2A′). We quantified this change in color by measuring the reflectance of the ridges and crossribs on upper surfaces manually isolated from the underlying LL—our microspectrophotometer set-up enabled us to measure a spot size between 1.1 and 1.2 μm (Figure S2). We found that the reflectance peak for the ridges and crossribs shifted toward blue wavelengths over the course of the experiment (Figures 2B and 2C). By measuring the height of ridges and crossribs from transverse and sagittal focused ion beam scanning electron micrograph (FIB-SEM) sections (Figure 2D), we also found that the height of both structures increased over the course of the experiment (Figures 2E and 2F). Similar trends were found for the thicknesses of the air layer below the ridges (Figure 2G) and crossribs (Figure 2H), as well as for the total height (chitin + air layer) of ridges (Figure 2I) and crossribs (Figure 2J). Lastly, we detected an increase in the mean distance between crossribs (d_{WT} = 862 ± 71 nm versus d_{G8} = 1160 ± 116 nm) (Figure S3B) (Tables S3 and S4), but not between ridges (Figure S3C). The increase in the distance between crossribs increased the mean window area (Figure S3D) ($area_{WT}$ = 0.72 ± 0.2 μm^2 versus $area_{G8}$ = 1.2 ± 0.3 μm^2) (Tables S3 and S4). These results suggest that artificial selection acted simultaneously on several components of the scale geometry: the LL thickness as previously identified,[15] but also the ridge and crossrib heights, as well as the spacing between crossribs (this study). These morphological changes all contribute to the color shift observed over several generations of artificial selection in *B. anynana*.

Scale ridge hue correlates with ridge height

To test if conclusions drawn from the *B. anynana* selection lines can be generalized to other species, we measured both ridge reflectance and geometries in the same 39 stereotypical scale types from the 34 species sampled above, but using intact scales. We first investigated how the ridge reflectance measurements made on the upper scale surface separated from the LL in *B. anynana* compared to those made in intact scales of the G8 generation (Figures S4A and S4B). The wavelength of peak light reflection was identical regardless of sampling strategy (Figure S4C), even though the intensity of the ridge reflectance is higher on the intact scale because the LL prevents the backscattering of white light. Furthermore, reflectance measurements centered on the ridge in intact scale (= ridge + LL) and on the isolated LL (LL only) had distinct wavelength peaks (Figure S4C), demonstrating that our microspectrophotometer enables the measurement of individual ridge reflectance. Measurements of ridge reflectance of all subsequent species were, therefore, done on intact scales. Under epi-illumination, ridges exhibited a continuum of colors ranging from violet to green (Figures 3A–3D). The morphology and the geometry of these colored ridges (and crossribs) varied substantially across scales (Figures 3A'–D′ and 3A''–D''), including cases where ridges and/or crossribs had the appearance of chitinous walls with almost no underlying air gaps.

Our analysis revealed that ridge hue strongly and positively correlated with ridge height, but this correlation was only visible when ridge height was broken down into two separate height intervals (Figure 4A). We ran phylogenetic generalized least squares (PGLS) to incorporate phylogenetic relatedness to account for non-independence of data points between the species in our sample. When the ridges were between 268 and 1036 nm in height, their color hue ranged from about 379 to 594 nm, with a

(B) Measured reflectance spectra of ridges over generations.
(C) Measured reflectance spectra of crossribs over generations. Graph colors were arbitrarily chosen: WT scales (brown), violet-blue line (generation G6) scales (purple), violet-blue line (generation G8) scales (blue). The arrowheads indicate the reflectance peaks.
(D) Schematic of a *B. anynana* ground scale showing how ridge, crossrib, and air layer heights were measured.
(E and F) Ridge and crossrib height over generations.
(G and H) Air layer thickness under the ridge and crossrib over generations.
(I and J) Total height over generations. Means sharing the same letter are not significantly different (Tukey-adjusted comparisons). The central line in the violin plot indicates the median of the distribution, while the top and bottom of the box represent the third and first quartiles of the data, respectively. The whiskers show up to 1.5 times the inter-quartile range.

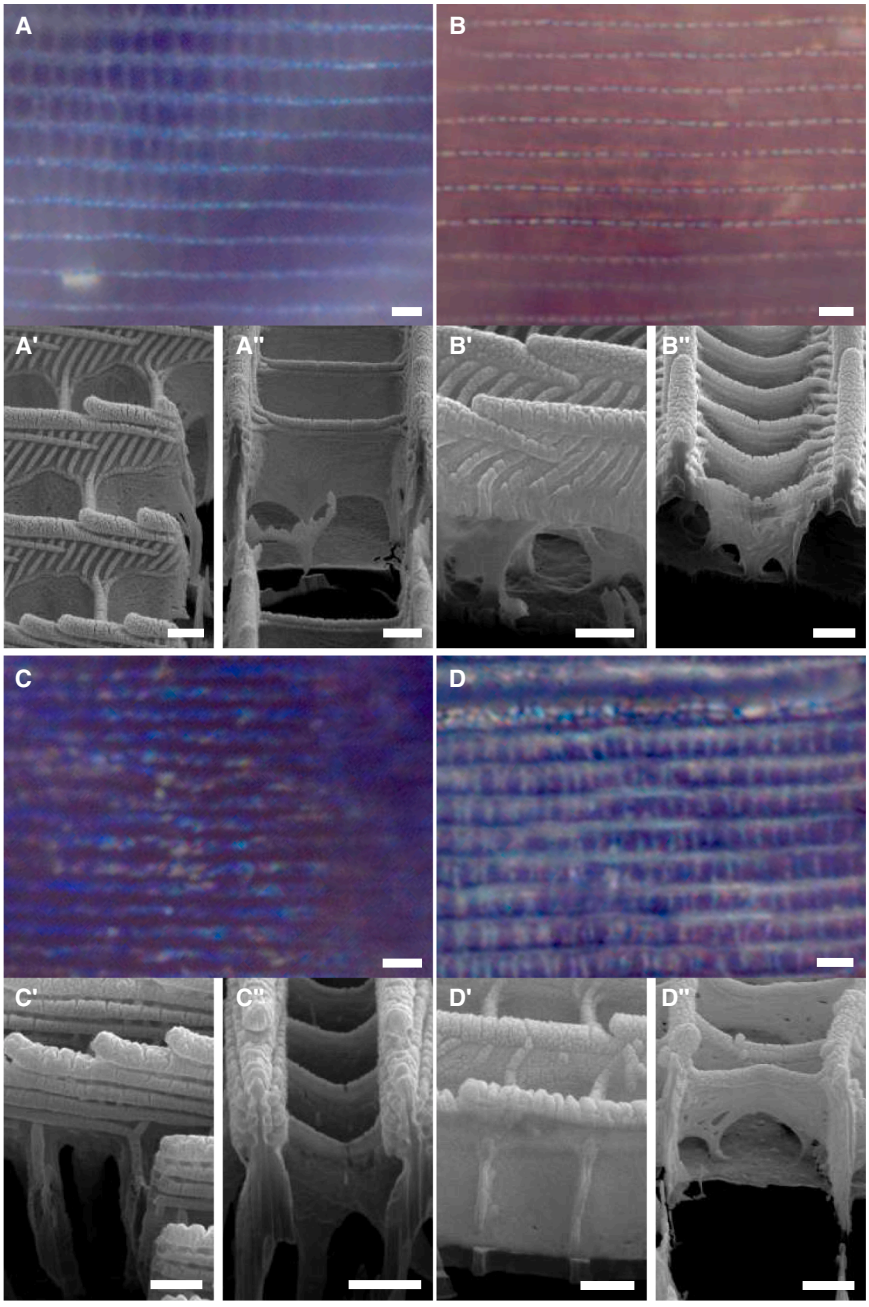

Figure 3. Diversity of ridge and crossrib structural coloration

Optical microscopy images of the abwing side of blue or green cover scales of (A) *Prothoe franck* (Nymphalidae), (B) *Pyrrhopyge hadassa* (Hesperiidae), (C) *Euploea mulciber* (Nymphalidae), and (D) *Paralaxita orphna* (Riodinidae).

(A′–D′) FIB-SEM images show a sagittal view of the scale. (A″–D″) FIB-SEM images showing a transverse view of the scale. Scale bars indicate 2 μm on optical microscopy images, and 500 nm on FIB-SEM images.

significant positive correlation (intercept: 117.13, β = 0.76, SE = 0.22, t = 3.51, p = 3.1e-03) (Figure 4B). As the ridge height continued to increase, the color sequence began again at cool blues and progressed to warmer hues. This positive correlation was very significant for taller ridges between 1126 and 2184 nm (intercept: −554.08, β = 4.57, SE = 0.40, t = 11.54, p < 1e-04) (Figure 4C).

The correlation between the ridge height and color hue can be explained by a previously published interference model,[39] in which two light waves propagate through the ridges and through the air next to the ridges (the windows), and interfere with each other when they exit either into the air gap below the ridges, or above the ridges, as light travels back via the same path after reflection from the LL of the scale. When the phase difference between the ridge path and the air path equals an even multiple of Pi (π), the constructive interference of the two waves gives rise to spectral peaks, whose wavelengths/hues (λ) are given by:

$$\lambda = \frac{2\left(n_{\text{ridge}} - n_{\text{air}}\right)}{i} h_{\text{ridge}}$$

where i is an arbitrary even number, h_{ridge} is the height of the ridge, and n_{ridge} and n_{air} are the refractive indices of chitin and air, respectively. The plots where i equals 2 and 4 (Figure 4D) represent the cases with the phase difference of 2π and 4π, and they fit the data points in Figures 4B and 4C, respectively. This model also predicts a third interval for ridges with the height higher than 1500 nm, which could correspond to our single data point in black (Figure 4A; *Cithaerias esmeralda*).

In addition to ridge height, other factors might impact ridge reflectance. First, pigments contained in the mass of the ridge could have a substantial role as frequency-dependent attenuators of optical signals. To test the contribution of pigments, we measured ridge reflectance in bleach-treated, depigmented scales. Qualitative and quantitative tests performed in *M. didius* showed that a 1-min bleach treatment is enough to cancel scale absorbance (Figure S5). Thus, we ran the experiment on all the available scales, and we found that the removal of pigments does not substantially affect the overall correlation between ridge height and ridge reflectance (Figure S6 and Table S5). The data points' positions only slightly changed, but the nearly vertical cluster of orange points near 410 nm disappeared after bleaching, indicating that it was likely attributed to pigmentary effects. Second, variation in ridge nanomorphology could also explain differences in ridge reflectance. The FIB-SEM sections

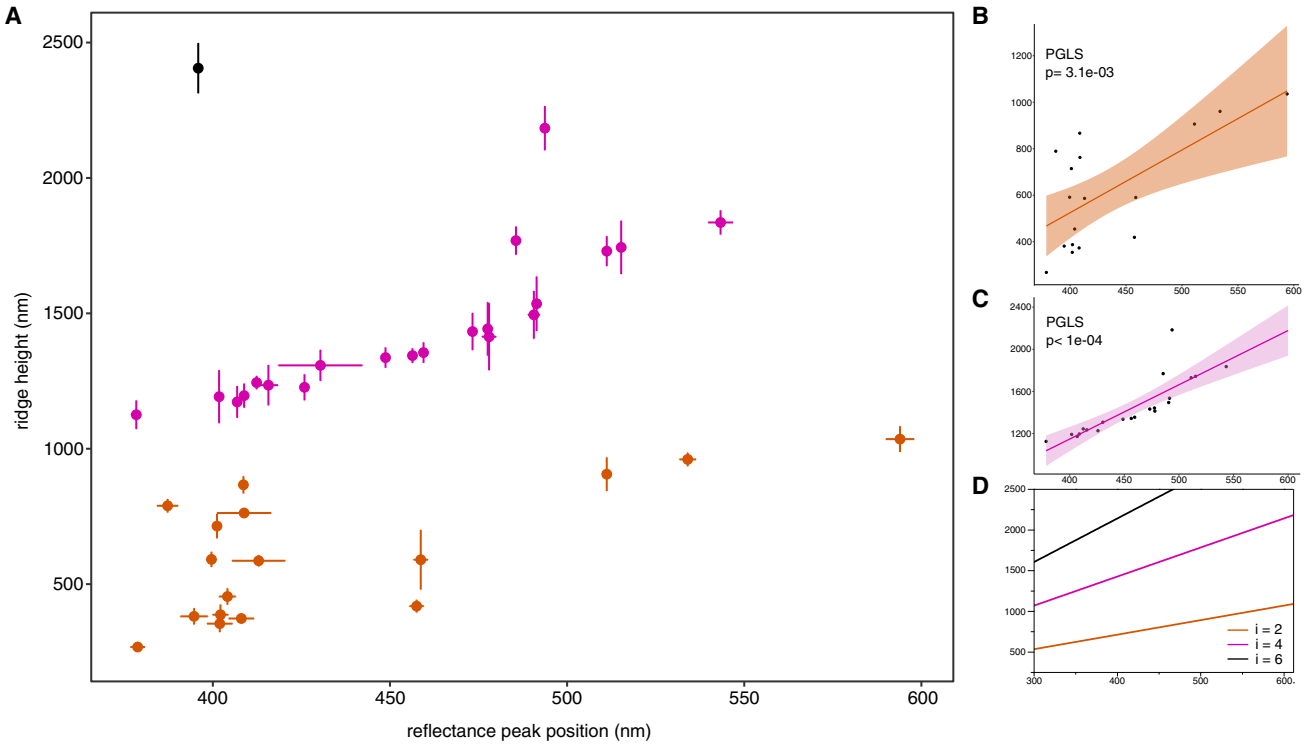

Figure 4. Correlation between ridge height and ridge color hue across species

(A) Scatterplot with error bars shows the whole dataset that includes 39 scales from 34 species (Table S1). Distinct colors were used to help visualize the different cohorts that belong to a different height category (step function): 268–1036 nm high ridges (orange), 1126–2184 nm high ridges (pink), and above 2184 nm high ridges (black).

(B) Linear regression and standard deviation for the subdataset that includes the shorter ridges (orange).

(C) Linear regression and standard deviation for the subdataset that includes the taller ridges (pink).

(D) Plots of peak wavelengths versus the ridge height according to the interference model where *i* equals 2, 4, and 6, respectively.

obtained for the 39 scale types demonstrate that the ridges are solid structures without the indication of internal structure, such as layering. However, ridge stacked lamellae were present in most of the scale types, although they are not as exaggerated in size as scales with *Morpho*-type Christmas-tree ridges. We found that their number varied between 1 and 11 (Table S6) and their spacing between 17 and 143 nm (Table S6). We plotted lamella number and lamella spacing as functions of reflectance, but we found no indication that these parameters correlate with ridge color (Figure S7).

Our findings imply that varying ridge heights can impart different colors to scales that are comparable in LL thickness and pigment content (see Table S7 for LL thicknesses in all the samples). This is exemplified in the scales of *Paralaxita orphna* and *Elymnias malelas*, which exhibit ridges that range in height from 590 to 1414 nm, have a similar LL thickness (~170 nm; Figures S8A and S8B), and show similar absorbance spectra from pigments largely localized in ridges (Figures S8A' and B′) but with slight differences in intensity (Figures S8A'' and B''). After bleach treatment, the relative ridge peak reflectance remained unchanged (Figures S6 and S8, and Table S5). These scales illustrate how changes strictly in the ridge height can affect the color of the upper lamina.

Experimental and simulation-based manipulation of ridge height impacts coloration

To go beyond correlations, we manipulated the ridge height in the nymphalid butterfly *Morpho didius* (Figures 5A and 5B). The current model for the metallic blue color of *M. didius* wings assumes that the spatial separation between the stacked lamellae—sometimes referred to as Christmas tree-like reflectors—that protrude from the sides of the ridges is the key structural feature that produces blue color.[8,40,41] The reflected light waves from consecutive lamellae interfere with each other so that the reflected blue wavelengths are intensified via constructive interference, whereas other wavelengths cancel each other out via destructive interference.

To test the role of ridge height in blue color generation, we performed a series of FIB-SEM millings of the full ridge (core + lamellae) of an uncoated scale at different depths (Figure 5C), followed by reflectance measurements. We found that the reflection spectrum was UV-shifted when the ridge height was decreased (Figure 5C'). This shift in hue was also accompanied by a progressive decrease in overall light reflected (Figure 5C'), which is in line with previous studies that show that stacked lamellae are the main reflectors in these scales.

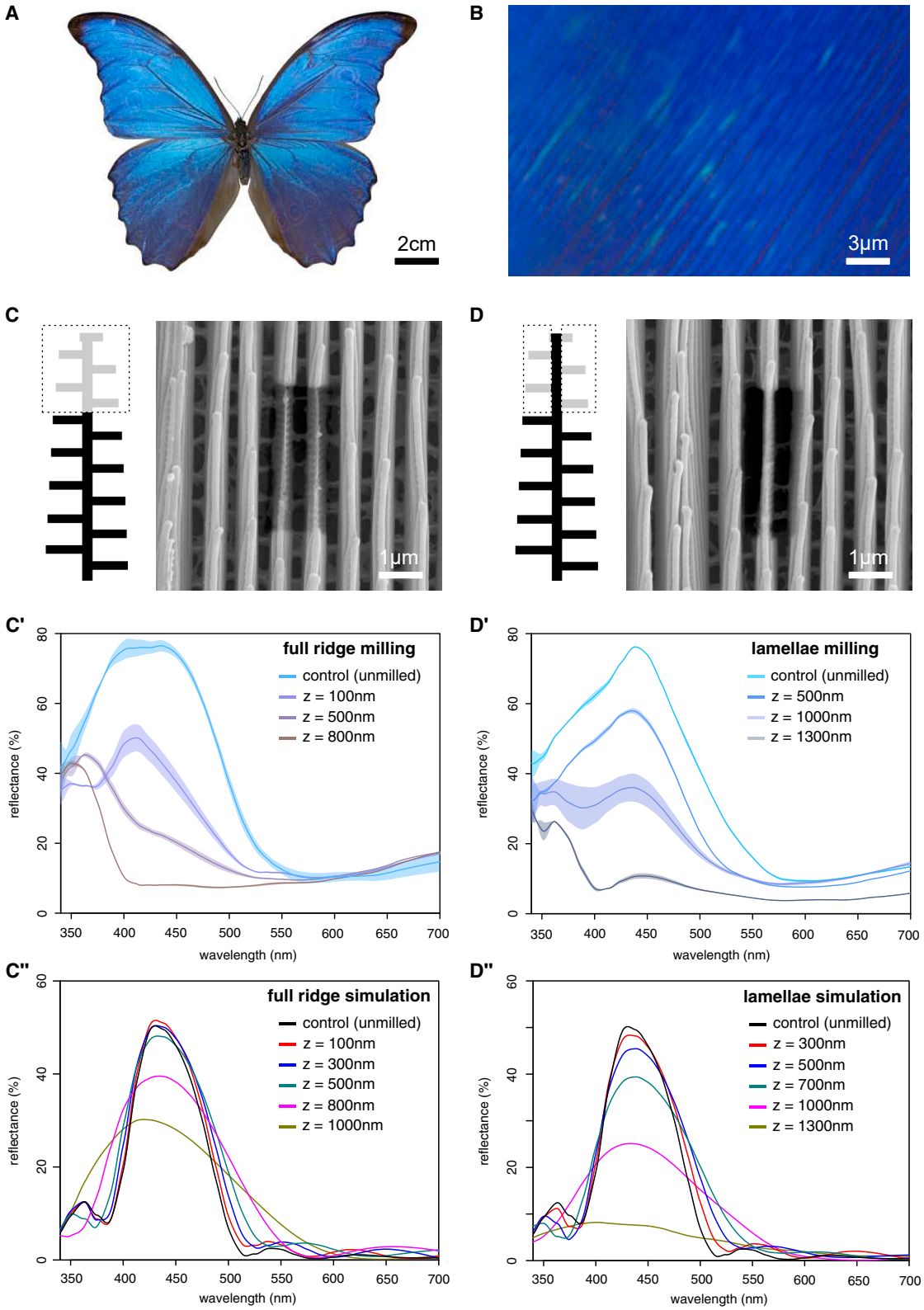

Figure 5. Testing the role of ridge height in *Morpho didius*

(A) Adult specimen of *M. didius* from Peru (photo: Didier Descouens, Muséum d'Histoire Naturelle de Toulouse, CC BY-SA 4.0).

(legend continued on next page)

A limitation of gallium ion milling lies in the implantation of ions up to tens of nanometers from the milled area, resulting in local variation in chitin thickness near the edge.[42] However, the use of low beam voltage and beam current is known to reduce this artifact.[43] We purposely used the gallium beam at 8 keV with a beam current of 12 pA (versus 30 keV with 100 pA in Allen et al.[42]). In addition, we performed a series of control experiments which demonstrate that the lateral spread of the Ga beam only affects the ridge immediately adjacent to the milled ridge—and not a wider region of the scale (Figure S9), and that the exposure times we used are too short to induce a color shift of the region surrounding the milling area (Figure S10). Last, to rule out that Ga itself shifts the color toward UV wavelengths, we milled the ridges in *Prothoe franck* at different depths (Figure S11). While a milling to a depth of z = 100 nm shifted the ridge peak reflectance toward UV, deeper millings (z = 500 and 1000 nm) shifted the peak toward longer wavelengths. Because we observed bi-directional changes in scale hue after FIB-SEM milling, we can conclude that Ga itself does not impact the sample hue.

To better understand how shortening ridges affects scale hue, we developed an optical model consisting of parallel ridges with lateral lamellae, with dimensions obtained from our SEM images of *M. didius* (Figure S12). The simulated reflectance shows a peak around 430 nm that matches the reflection measured for the ridge in real scales (Figure 5D''). Shortening the ridge height showed a shift toward shorter (UV) wavelengths as the full ridge shortened by 800–1000 nm (Figure 5C''). However, our model was not sensitive enough to capture a shift for milder milling by 100–500 nm (Figure 5C''). In summary, both our experimental and *in silico* data show that changes in ridge height alter color hue, and suggest that the height of the central, core part of the ridge alone might control the blue color in *M. didius*.

To disentangle the relative roles of ridge elements further, we selectively removed ridge lamellae from both sides of a single ridge at different depths by FIB milling (Figure 5D). We found that the position of the reflectance peak (~430 nm) remained unchanged regardless of the depth of milling (Figure 5D'), but light reflection was drastically reduced, being halved by milling to a depth of z = 1000 nm (Figure 5D'). We confirmed these results in our model by varying the height of the lamellar stack while keeping constant the height of the core part of the ridge (Figure 5D''). Similarly, we found that the height of the stack of lamellae is crucial for brilliance and saturation, as previously shown.[40,41,44] In summary, the height of the central, core part of the ridge, and the ridge lamella both seem to be tuned to produce the overall structural blue color of *M. didius*, with the lamellar layers considerably increasing the brightness of the reflected blue light, and hue being affected by manipulations of both traits, but not by the number of lamella alone.

DISCUSSION

Our findings show that height variations in the ridges and crossribs of a stereotypical scale are an ''evolutionary accessible'' route to alter the scale's structural color. This new optical mechanism adds to the previously identified mechanisms, such as changes in the LL thickness and in the number and spacing of ridge lamellae.

First, our study of the artificially selected blue scales of *B. anynana* showed that ridge and crossrib height and (to a lesser extent), the airgap height beneath these structures all contributed to the generation of the blue scale hue, previously ascribed solely to changes in LL thickness.[15]

Second, by revealing a general law between ridge height and color hue, our findings shed new light on a new causative mechanism of structurally colored ridges across nymphalids,[22,23,40,45,46] pierids,[47,48] and lycaenid butterflies.[49] In many of these species, the ridges have a Christmas-tree-like, or Morpho type, structure,[8,50] whose prominent side lamella was thought to be the main color-generating features.[8,40,41,44,51] However, our comparative analyses, ridge manipulative experiments, and modeling work propose that ridge coloration is produced both by ridge height and independently from ridge lamella, where the precisely spaced stacked lamellae could be amplifying a corresponding structural hue produced by ridge height.

The optical phenomenon that underlies ridge coloration differs from thin-film interference known to take place in the LL. This phenomenon has already been observed and modeled in the lab using non-biological, synthetic nanomaterials. Engineered ridge-like nanostructures made of transparent chitosan produced the entire structural color palette via variations in height alone.[25] The proposed model posits that the structural color coming from the ridges is not due to light interference from reflections produced at the top and bottom of the ridge, as observed in a thin film of chitin. Instead, the color results from interference between light that is weakly guided inside ridge, and light that travels in between consecutive ridges. In other words, light travels more slowly inside the chitinous ridges compared to light traveling on the outside of the ridges.[39] We propose that the same optical phenomenon might occur in the wing scale's ridges, offering a striking example of how synthetic biology aided our understanding of natural materials, such as butterfly scales.

Third, we have shown that the addition of an upper surface can either increase or decrease a scale's brilliance, and this may have selective consequences. In cases where a scale's natural brilliance has been subdued, which often happens in ventral surfaces of butterfly wings,[52,53] we hypothesize that this evolved for better camouflage and protection from predators, even though iridescence itself can sometimes serve as camouflage in other insects.[54,55] In cases where the upper surface makes scales brighter, as in the case of *Morpho* butterflies,[24] we hypothesize

(B) Epi-illumination of the wing showing the blue colored ridges (magnification 100×).
(C) SEM top view of scale after milling of two consecutive ridges (core + lamellae). (C′) Measured reflectance of intact and milled ridges at different depths. (C″) Simulated reflectance of intact and milled ridges at different depths.
(D) SEM top view of scale after milling of lateral lamellae of the same ridge. (D′) Measured reflectance of intact and milled lamellae at different depths. (D″) Simulated reflectance of intact and milled lamellae at different depths.

that this evolved for purposes of sexual signaling[40] and/or to confuse predators by signaling unprofitability, such as unpalatability[56] and reduced capture success via motion dazzle effect.[57]

Beyond their biological significance, the optical mechanisms revealed in this study hold broad technological relevance. Structural colors generated by well-defined micro- and nanostructures have attracted increasing attention for pigment-free colorants due to their exceptional brightness, long-term photostability, and environmental sustainability.[58,59] The optical responses of the ridge-based microstructures could also offer promising routes for anti-counterfeiting tags and secure optical encryption.[60,61] In addition, butterfly inspired photonic architectures have facilitated the development of highly sensitive optical sensors for strain, humidity, and chemical analytes.[62,63] A deeper understanding of how ridges and lamina contribute to color formation, therefore, not only enriches our knowledge of developmental and evolutionary mechanisms but also guides the rational design of multifunctional photonic materials for diverse technological applications.

Limitations of the study

In this study, ridge and crossrib reflectance were measured by collecting light scattered back from small areas, which are prone to increased data noise. We overcame this issue by using three replicates per sample and extracting values from smoothed curves, which is the standard practice for most published spectral data. In addition, reflectance was measured under normal incident light and lacks angle-dependent information. Yet, some studies have shown that lepidopteran scales can be highly iridescent, i.e., their color changes with the angle of incidence of light and the viewing angle of an observer.[22,40,47,64–68] Furthermore, butterflies and moths use the high directionality of iridescent colors for communicating[40,57,69] and maximizing conspicuousness.[70–72] Angle-dependent reflectance should be considered in future studies.

Another limitation is the way we assumed that ridges were uniform in chitin density. Even if the FIB-SEM cross-sections did not show signs of heterogeneities in chitin density, contrary to what has been recently observed in the LL,[73] transmission electron microscopy might be a finer and more appropriate method to detect such heterogeneities in the deposition of chitin and other cuticular components such as pigments.

Finally, while FIB-SEM is routinely used to measure geometrical parameters of wing scales,[16,19,31,46,73–77] this approach introduces uncertainties due to the complex 3D morphology of the wing scale, image distortion, and platinum coating. Prior to FIB-SEM milling, we mounted the scales as flat as possible on the stub and looked for color heterogeneity under epi-illumination, which could indicate unusually "bumpy" samples. For FIB milling, the sample is tilted near the 52° angle of the Gallium ion column so the ion beam can mill a trench or expose a cross-section. The SEM camera then views this tilted, milled surface from its own fixed angle. This angled viewing causes foreshortening and perspective shifts. We corrected for image distortion using the geometrical correction thickness/sin52°. Regarding any potential overestimation owing to platinum coating, the stark contrast between the platinum coating and the scale tissue allowed us to exclude the thickness of the platinum layer from our measurements.

RESOURCE AVAILABILITY

Lead contact

Further information and requests for resources should be directed to and will be fulfilled by the Lead contact, Cédric Finet (cedric.finet@ens-lyon.org).

Materials availability

This study did not generate unique reagents.

Data and code availability

Data

Measured and simulated reflectance and absorbance spectra, measurements of scale geometries, nucleotide alignments, and phylogenetic trees have been deposited in Dryad (https://datadryad.org/share/Up0r8AmL-aeoeXaP6-POl6uRGfODHdl_68cz0d4LkWDg).

Code

This paper does not report original code.

Other items

Any additional information required to reanalyze the data reported in this paper is available from the lead contact upon request.

ACKNOWLEDGMENTS

We thank Michael Greeff (ETH Zürich), Rodolphe Rougerie (MNHN Paris), and Wei Song Hwang (LKCHM, NUS) for access to entomological collections; Anupama Prakash for help with statistical analyses; Javier Fernandez (SUTD), Joel Yang (SUTD), and Duane Loh (NUS) for discussions, and the Electron Microscopy Facility (EMF, NUS) for use of FIB-SEM. This project was supported by the National Research Foundation (NRF) Singapore, under the Competitive Research Program award NRF-CRP20-2017-0001 to A.M. and V.S. Q.F.R acknowledges the National Natural Science Foundation of China (no. 12304415), the Guangdong Provincial Quantum Science Strategic Initiative (GDZX2306002), and the Guangdong Pearl River Talent Program (2023QN10X058).

AUTHOR CONTRIBUTIONS

Conceptualization: C.F., Q.R., and A.M.; formal analysis: C.F. and Q.R.; funding acquisition: V.S. and A.M.; investigation: C.F., Q.R., and Y.Y.B.; methodology: C.F., Q.R., V.S., and A.M.; supervision: C.F. and A.M.; validation: C.F.; visualization: C.F.; writing – original draft: C.F., Q.R., and A.M.; writing – review and editing: C.F., Q.R., Y.Y.B., V.S., and A.M.

DECLARATION OF INTERESTS

The authors declare no competing interests.

STAR★METHODS

Detailed methods are provided in the online version of this paper and include the following:

- Color quantification
- Statistical analysis

SUPPLEMENTAL INFORMATION

Supplemental information can be found online at https://doi.org/10.1016/j.isci.2026.115374.

Received: September 3, 2025
Revised: January 26, 2026
Accepted: March 12, 2026
Published: March 16, 2026

REFERENCES

1. Srinivasarao, M. (1999). Nano-Optics in the Biological World: Beetles, Butterflies. Birds, and Moths. Chem. Rev. *99*, 1935–1961. https://doi.org/10.1021/cr970080y.
2. Vukusic, P., and Sambles, J.R. (2003). Photonic structures in biology. Nature *424*, 852–855. https://doi.org/10.1038/nature01941.
3. Airoldi, C.A., Ferria, J., and Glover, B.J. (2019). The cellular and genetic basis of structural colour in plants. Curr. Opin. Plant Biol. *47*, 81–87. https://doi.org/10.1016/j.pbi.2018.10.002.
4. Ghiradella, H. (1991). Light and color on the wing: structural colors in butterflies and moths. Appl. Opt. *30*, 3492–3500. https://doi.org/10.1364/ao.30.003492.
5. Vukusic, P., and Sambles, R. (2000). Colour effects in bright butterflies. J. Soc. Dyers Colour. *116*, 376–380.
6. Vukusic, P., Sambles, J.R., and Ghiradella, H. (2000). Optical classification of microstructure in butterfly wing-scales. Photonics Sci. News *6*, 61–66.
7. Downey, J., and Allyn, A. (1975). Wing-scale morphology and nomenclature. Bull. Allyn Mus. *31*, 1–32.
8. Ghiradella, H. (1984). Structure of Iridescent Lepidopteran Scales: Variations on Several Themes1. Ann. Entomol. Soc. Am. *77*, 637–645. https://doi.org/10.1093/aesa/77.6.637.
9. Ghiradella, H. (1985). Structure and Development of Iridescent Lepidopteran Scales: the Papilionidae as a Showcase Family. Ann. Entomol. Soc. Am. *78*, 252–263. https://doi.org/10.1093/aesa/78.2.252.
10. Thayer, R., and Patel, N.H. (2023). A meta-analysis of butterfly structural colors: their color range, distribution and biological production. J. Exp. Biol. *226*, jeb245940. https://doi.org/10.1242/jeb.245940.
11. Ghiradella, H. (1989). Structure and development of iridescent butterfly scales: Lattices and laminae. J. Morphol. *202*, 69–88. https://doi.org/10.1002/jmor.1052020106.
12. Ghiradella, H. (2010). Insect cuticular surface modifications: scales and other structural formations. In Advances in Insect Physiology, J. Casas and S.J. Simpson, eds. (Elsevier Ltd), pp. 135–180.
13. Yeh, P. (2005). Optical waves in layered media (Wiley-Interscience).
14. Stavenga, D.G., Leertouwer, H.L., and Wilts, B.D. (2014). Coloration principles of nymphaline butterflies - Thin films, melanin, ommochromes and wing scale stacking. J. Exp. Biol. *217*, 2171–2180. https://doi.org/10.1242/jeb.098673.
15. Wasik, B.R., Liew, S.F., Lilien, D.A., Dinwiddie, A.J., Noh, H., Cao, H., and Monteiro, A. (2014). Artificial selection for structural color on butterfly wings and comparison with natural evolution. Proc. Natl. Acad. Sci. USA *111*, 12109–12114. https://doi.org/10.1073/pnas.1402770111.
16. Thayer, R., Allen, F., and Patel, N.H. (2020). Structural color in Junonia butterflies evolves by tuning scale lamina thickness. eLife *9*, e52187. https://doi.org/10.7554/eLife.52187.
17. Bálint, Z., Katona, G., Sáfián, S., Collins, S., Piszter, G., Kertész, K., and Biró, L.P. (2023). Measuring and Modelling Structural Colours of Euphaedra neophron (Lepidoptera: Nymphalidae) Finely Tuned by Wing Scale Lower Lamina in Various Subspecies. Insects *14*, 303. https://doi.org/10.3390/insects14030303.
18. Stavenga, D.G., Matsushita, A., Arikawa, K., Leertouwer, H.L., and Wilts, B.D. (2012). Glass scales on the wing of the swordtail butterfly Graphium sarpedon act as thin film polarizing reflectors. J. Exp. Biol. *215*, 657–662. https://doi.org/10.1242/jeb.066902.
19. Finet, C., Ruan, Q., Bei, Y.Y., You En Chan, J., Saranathan, V., Yang, J.K.W., and Monteiro, A. (2023). Multi-scale dissection of wing transparency in the clearwing butterfly Phanus vitreus. J. R. Soc. Interface *20*, 20230135. https://doi.org/10.1098/rsif.2023.0135.
20. Zhang, Q., Mey, W., Ansorge, J., Starkey, T.A., McDonald, L.T., McNamara, M.E., Jarzembowski, E.A., Wichard, W., Thomson, U., Ren, X., et al. (2018). Fossil scales illuminate the early evolution of lepidopterans and structural colors. Sci. Adv. *4*, e1700988. https://doi.org/10.1126/sciadv.1700988.
21. Kilchoer, C., Steiner, U., and Wilts, B.D. (2019). Thin-film structural coloration from simple fused scales in moths. Interface Focus *9*, 20180044. https://doi.org/10.1098/rsfs.2018.0044.
22. Brink, D.J., and Lee, M.E. (1999). Confined blue iridescence by a diffracting microstructure: an optical investigation of the Cynandra opis butterfly. Appl. Opt. *38*, 5282–5289. https://doi.org/10.1364/ao.38.005282.
23. Stavenga, D.G., Leertouwer, H.L., and Arikawa, K. (2020). Coloration principles of the Great purple emperor butterfly (Sasakia charonda). Zool. Lett. *6*, 13. https://doi.org/10.1186/s40851-020-00164-6.
24. Giraldo, M.A., and Stavenga, D.G. (2016). Brilliant iridescence of Morpho butterfly wing scales is due to both a thin film lower lamina and a multilayered upper lamina. J. Comp. Physiol. *202*, 381–388. https://doi.org/10.1007/s00359-016-1084-1.
25. Raut, H.K., Ruan, Q., Finet, C., Saranathan, V., Yang, J.K.W., and Fernandez, J.G. (2022). The Height of Chitinous Ridges Alone Produces the Entire Structural Color Palette. Adv. Mater. Interfaces *9*, 2201419. https://doi.org/10.1002/admi.202201419.
26. Espeland, M., Breinholt, J., Willmott, K.R., Warren, A.D., Vila, R., Toussaint, E.F.A., Maunsell, S.C., Aduse-Poku, K., Talavera, G., Eastwood, R., et al. (2018). A Comprehensive and Dated Phylogenomic Analysis of Butterflies. Curr. Biol. *28*, 770–778.e5. https://doi.org/10.1016/j.cub.2018.01.061.
27. Simonsen, T.J. (2007). Comparative morphology and evolutionary aspects of the reflective under wing scale-pattern in Fritillary butterflies (Nymphalidae: Argynnini). Zool. Anz. *246*, 1–10. https://doi.org/10.1016/j.jcz.2005.04.005.
28. Vukusic, P., Kelly, R., and Hooper, I. (2009). A biological sub-micron thickness optical broadband reflector characterized using both light and microwaves. J. R. Soc. Interface *6*, S193–S201. https://doi.org/10.1098/rsif.2008.0345.focus.
29. Wilts, B.D., Pirih, P., Arikawa, K., and Stavenga, D.G. (2013). Shiny wing scales cause spec(tac)ular camouflage of the angled sunbeam butterfly, Curetis acuta. Biol. J. Linn. Soc. *109*, 279–289. https://doi.org/10.1111/bij.12070.
30. Ren, A., Day, C.R., Hanly, J.J., Counterman, B.A., Morehouse, N.I., and Martin, A. (2020). Convergent Evolution of Broadband Reflectors Underlies Metallic Coloration in Butterflies. Front. Ecol. Evol. *8*, 206. https://doi.org/10.3389/fevo.2020.00206.
31. Prakash, A., Finet, C., Banerjee, T.D., Monteiro, A., Saranathan, V., and Monteiro, A. (2022). Antennapedia and optix regulate metallic silver wing scale development and cell shape in Bicyclus anynana butterflies. Cell Rep. *40*, 111052.
32. Mason, C.W. (1927). Structural colors in insects. J. Phys. Chem. *31*, 321–354.
33. Biró, L.P., Kertész, K., Vértesy, Z., Márk, G.I., Bálint, Z., Lousse, V., and Vigneron, J.P. (2007). Living photonic crystals: Butterfly scales - Nanostructure and optical properties. Mater. Sci. Eng. C *27*, 941–946. https://doi.org/10.1016/j.msec.2006.09.043.

34. Michielsen, K., and Stavenga, D.G. (2008). Gyroid cuticular structures in butterfly wing scales: Biological photonic crystals. J. R. Soc. Interface *5*, 85–94. https://doi.org/10.1098/rsif.2007.1065.

35. Wilts, B.D., Ijbema, N., and Stavenga, D.G. (2014). Pigmentary and photonic coloration mechanisms reveal taxonomic relationships of the Cattlehearts (Lepidoptera: Papilionidae: Parides). BMC Evol. Biol. *14*, 160. https://doi.org/10.1186/s12862-014-0160-9.

36. Lukhtanov, V.A., Kandul, N.P., Plotkin, J.B., Dantchenko, A.V., Haig, D., and Pierce, N.E. (2005). Reinforcement of pre-zygotic isolation and karyotype evolution in Agrodiaetus butterflies. Nature *436*, 385–389. https://doi.org/10.1038/nature03704.

37. White, T.E., Macedonia, J., Birch, D., Dawes, J., and Kemp, D.J. (2012). The nanoanatomical basis of sexual dimorphism in iridescent butterfly colouration. Aust. J. Zool *60*, 101–107. https://doi.org/10.1071/ZO12045.

38. Giraldo, M.A., Yoshioka, S., Liu, C., and Stavenga, D.G. (2016). Coloration mechanisms and phylogeny of Morpho butterflies. J. Exp. Biol. *219*, 3936–3944. https://doi.org/10.1242/jeb.148726.

39. Ruan, Q., Zhang, W., Wang, H., Chan, J.Y.E., Wang, H., Liu, H., Fan, D., Li, Y., Qiu, C.W., and Yang, J.K.W. (2022). Reconfiguring Colors of Single Relief Structures by Directional Stretching. Adv. Mater. *34*, e2108128. https://doi.org/10.1002/adma.202108128.

40. Vukusic, P., Sambles, J.R., Lawrence, C.R., and Wootton, R.J. (1999). Quantified interference and diffraction in single Morpho butterfly scales. Proc. R. Soc. Lond. B. *266*, 1403. https://doi.org/10.1098/rspb.1999.0794.

41. Kinoshita, S., Yoshioka, S., Fujii, Y., and Okamoto, N. (2002). Photophysics of Structural Color in the Morpho Butterflies. Forma *17*, 103–121.

42. Allen, F.I., Velez, N.R., Thayer, R.C., Patel, N.H., Jones, M.A., Meyers, G.F., and Minor, A.M. (2019). Gallium, neon and helium focused ion beam milling of thin films demonstrated for polymeric materials: Study of implantation artifacts. Nanoscale *11*, 1403–1409. https://doi.org/10.1039/c8nr08224c.

43. Bals, S., Tirry, W., Geurts, R., Yang, Z., and Schryvers, D. (2007). High-quality sample preparation by low kV FIB thinning for analytical TEM measurements. Microsc. Microanal. *13*, 80–86. https://doi.org/10.1017/S1431927607070018.

44. Gralak, B., Tayeb, G., and Enoch, S. (2001). Morpho butterflies wings color modeled with lamellar grating theory. Opt. Express *9*, 567–578. https://doi.org/10.1364/oe.9.000567.

45. Ćurčić, S.B., Pantelić, D.V., Ćurčić, B.P.M., Savić-Šević, S.N., Makarov, S.E., Lačković, V.B., Labudović-Borović, M.M., Ćurčić, N.B., and Stojanović, D.V. (2012). Micro- and nanostructures of iridescent wing scales in purple emperor butterflies (Lepidoptera: Apatura ilia and A. iris). Microsc. Res. Tech. *75*, 968–976. https://doi.org/10.1002/jemt.22021.

46. Parnell, A.J., Bradford, J.E., Curran, E.V., Washington, A.L., Adams, G., Brien, M.N., Burg, S.L., Morochz, C., Fairclough, J.P.A., Vukusic, P., et al. (2018). Wing scale ultrastructure underlying convergent and divergent iridescent colours in mimetic Heliconius butterflies. J. R. Soc. Interface *15*, 20170948. https://doi.org/10.1098/rsif.2017.0948.

47. Ghiradella, H., Aneshansley, D., Eisner, T., Silberglied, R.E., and Hinton, H.E. (1972). Ultraviolet reflection of a male butterfly: Interference color caused by thin-layer elaboration of wing scales. Science *178*, 1214–1217. https://doi.org/10.1126/science.178.4066.1214.

48. Stavenga, D.G., Giraldo, M.A., and Hoenders, B.J. (2006). Reflectance and transmittance of light scattering scales stacked on the wings of pierid butterflies. Opt. Express *14*, 4880–4890. https://doi.org/10.1364/oe.14.004880.

49. Tilley, R., and Eliot, J. (2002). Scale microstructure and its phylogenetic implications in lycaenid butterflies (Lepidoptera, Lycaenidae). Trans. Lepidopterol. Soc. Japan *53*, 153–180.

50. Lippert, W., and Gentil, K. (1959). Über lamellare feinstrukturen bei den schillerschuppen der schmetterlinge vom urania- und morpho-typ. Zeitschrift für Morphol. Z. Morph. u. Okol. Tiere *48*, 115–122. https://doi.org/10.1007/BF00407836.

51. Tabata, H., Kumazawa, K., Funakawa, M., Takimoto, J.I., and Akimoto, M. (1996). Microstructures and optical properties of scales of butterfly wings. Opt. Rev. *3*, 139–145. https://doi.org/10.1007/s10043-996-0139-x.

52. Oliver, J.C., Robertson, K.A., and Monteiro, A. (2009). Accommodating natural and sexual selection in butterfly wing pattern evolution. Proc. Biol. Sci. *276*, 2369–2375. https://doi.org/10.1098/rspb.2009.0182.

53. Allen, C.E., Zwaan, B.J., and Brakefield, P.M. (2011). Evolution of sexual dimorphism in the lepidoptera. Annu. Rev. Entomol. *56*, 445–464. https://doi.org/10.1146/annurev-ento-120709-144828.

54. Kjernsmo, K., Hall, J.R., Doyle, C., Khuzayim, N., Cuthill, I.C., Scott-Samuel, N.E., and Whitney, H.M. (2018). Iridescence impairs object recognition in bumblebees. Sci. Rep. *8*, 8095. https://doi.org/10.1038/s41598-018-26571-6.

55. Kjernsmo, K., Whitney, H.M., Scott-Samuel, N.E., Hall, J.R., Knowles, H., Talas, L., and Cuthill, I.C. (2020). Iridescence as Camouflage. Curr. Biol. *30*, 551–555.e3. https://doi.org/10.1016/j.cub.2019.12.013.

56. Pinheiro, C.E.G., Freitas, A.V.L., Campos, V.C., DeVries, P.J., and Penz, C.M. (2016). Both Palatable and Unpalatable Butterflies Use Bright Colors to Signal Difficulty of Capture to Predators. Neotrop. Entomol *45*, 107–113. https://doi.org/10.1007/s13744-015-0359-5.

57. Le Roy, C., Amadori, D., Charberet, S., Windt, J., Muijres, F.T., Llaurens, V., and Debat, V. (2021). Adaptive evolution of flight in Morpho butterflies. Science *374*, 1158–1162. https://doi.org/10.1126/science.abh2620.

58. Daqiqeh Rezaei, S., Dong, Z., You En Chan, J., Trisno, J., Ng, R.J.H., Ruan, Q., Qiu, C.W., Mortensen, N.A., and Yang, J.K.W. (2021). Nanophotonic Structural Colors. ACS Photonics *8*, 18–33. https://doi.org/10.1021/acsphotonics.0c00947.

59. Li, Y., Hu, J., Zeng, Y., Song, Q., Qiu, C.-W., and Xiao, S. (2024). Recent progress on structural coloration. Photonics Insights *3*, R03. https://doi.org/10.3788/PI.2024.R03.

60. Chan, J.Y.E., Ruan, Q., Wang, H., Wang, H., Liu, H., Yan, Z., Qiu, C.W., and Yang, J.K.W. (2022). Full Geometric Control of Hidden Color Information in Diffraction Gratings under Angled White Light Illumination. Nano Lett. *22*, 8189–8195. https://doi.org/10.1021/acs.nanolett.2c02741.

61. Liu, X., Sun, P., Wang, Y., Yuan, C., Hu, H., and Zheng, Z.-G. (2025). Orthogonal three-dimensional manipulation of a chiro-photonic hybrid-architecture enabling high-order information encryption. Mater. Horiz. *12*, 5654–5665.

62. Wang, J., Yu, H., Zheng, J., Zhang, Y., Guo, H., Qiu, Y., Wang, X., Yang, Y., and Liu, L. (2024). Nanograting-Based Dynamic Structural Colors Using Heterogeneous Materials. Nano-Micro Lett. *17*, 59.

63. Zhang, R., Zhao, H., Li, N., Chen, Y., Hu, Y., Zhang, Q., Chen, X., Ruan, Q., Long, Y., and Ke, Y. (2025). Mechanochromic Materials: From Principles, Multi-Mode Integration, to Emerging Applications. Adv. Funct. Mater. *36*, e21287. https://doi.org/10.1002/adfm.202521287.

64. Brink, D.J., Smit, J.E., Lee, M.E., and Möller, A. (1995). Optical diffraction by the microstructure of the wing of a moth. Appl. Opt. *34*, 6049–6057. https://doi.org/10.1364/ao.34.006049.

65. Tada, H., Mann, S.E., Miaoulis, I.N., and Wong, P.Y. (1998). Effects of a butterfly scale microstructure on the iridescent color observed at different angles. Appl. Opt. *37*, 1579–1584. https://doi.org/10.1364/ao.37.001579.

66. Kemp, D.J., Vukusic, P., and Rutowski, R.L. (2006). Stress-mediated covariance between nano-structural architecture and ultraviolet butterfly coloration. Funct. Ecol. *20*, 282–289. https://doi.org/10.1111/j.1365-2435.2006.01100.x.

67. Rutowski, R.L., Macedonia, J.M., Merry, J.W., Morehouse, N.I., Yturralde, K., Taylor-Taft, L., Gaalema, D., Kemp, D.J., and Papke, R.S. (2007). Iridescent ultraviolet signal in the orange sulphur butterfly (Colias eurytheme): Spatial, temporal and spectral properties. Biol. J. Linn. Soc. *90*, 349–364. https://doi.org/10.1111/j.1095-8312.2007.00749.x.

68. Siddique, R.H., Gomard, G., and Hölscher, H. (2015). The role of random nanostructures for the omnidirectional anti-reflection properties of the glasswing butterfly. Nat. Commun. Now. *6*, 1–8. https://doi.org/10.1038/ncomms7909.

69. White, T.E., Zeil, J., and Kemp, D.J. (2015). Signal design and courtship presentation coincide for highly biased delivery of an iridescent butterfly mating signal. Evolution *69*, 14–25. https://doi.org/10.1111/evo.12551.

70. Stavenga, D.G., Stowe, S., Siebke, K., Zeil, J., and Arikawa, K. (2004). Butterfly wing colours: Scale beads make white pierid wings brighter. Proc. Biol. Sci. *271*, 1577–1584. https://doi.org/10.1098/rspb.2004.2781.

71. Prum, R.O., Quinn, T., and Torres, R.H. (2006). Anatomically diverse butterfly scales all produce structural colours by coherent scattering. J. Exp. Biol. *209*, 748–765. https://doi.org/10.1242/jeb.02051.

72. Wijnen, B., Leertouwer, H.L., and Stavenga, D.G. (2007). Colors and pterin pigmentation of pierid butterfly wings. J. Insect Physiol. *53*, 1206–1217. https://doi.org/10.1016/j.jinsphys.2007.06.016.

73. Balakrishnan, D., Prakash, A., Daurer, B.J., Finet, C., Lim, Y.C., Shen, Z., Thibault, P., Monteiro, A., and Duane Loh, N. (2025). Nanoscale cuticle mass density variations influenced by pigmentation in butterfly wing scales. Nat. Commun. *16*, 7085. https://doi.org/10.1038/s41467-025-62010-7.

74. Banerjee, T.D., Monteiro, A., Finet, C., Seah, K.S., and Monteiro, A. (2024). Optix regulates nanomorphology of butterfly scales primarily via its effects on pigmentation. Front. Ecol. Evol. *12*, 1392050.

75. Ru, H., Finet, C., and Monteiro, A. (2025). Calreticulin is required for cuticle deposition and trabeculae formation inside butterfly wing scale cells. Dev. Biol. *526*, 1–14. https://doi.org/10.1016/j.ydbio.2025.06.013.

76. Chatterjee, M., Finet, C., Siegel, K.J., Tian, S., Zhou, Y.J., Loh, L.S., Yu, X.Y., Delgado, S., McDonald, J.M.C., Markenscoff-Papadimitriou, E., et al. (2026). araucan regulates butterfly wing iridescence by coordinating scle structure and pigmentation. Preprint at bioRxiv. https://doi.org/10.1101/2023.11.21.568172.

77. Finet, C., Weng, Y., Hanotte, B., and Monteiro, A. (2026). UV wing patterns in saturniid moths: diversity and mechanisms. J. Exp. Biol. *229*, jeb251600. https://doi.org/10.1242/jeb.251600.

78. Maia, R., Gruson, H., Endler, J.A., and White, T.E. (2019). pavo 2: New tools for the spectral and spatial analysis of colour in r. Methods Ecol. Evol. *10*, 1097–1107. https://doi.org/10.1111/2041-210X.13174.

79. Guindon, S., Dufayard, J.-F., Lefort, V., Anisimova, M., Hordijk, W., and Gascuel, O. (2010). New algorithms and methods to estimate maximum-likelihood phylogenies: assessing the performance of PhyML 3.0. Syst. Biol. *59*, 307–321. https://doi.org/10.1093/sysbio/syq010.

80. Oppenheim, A.V., Willsky, A.S., and Nawab, S.H. (1997). Signals & Systems 2nd Edition. (Prentice-Hall, Inc.).

81. R Core Team (2021). R: a language and environment for statistical computing (Vienna, Austria: R Foundation for Statistical Computing). https://www.R-project.org/.

82. Schindelin, J., Arganda-Carreras, I., Frise, E., Kaynig, V., Longair, M., Pietzsch, T., Preibisch, S., Rueden, C., Saalfeld, S., Schmid, B., et al. (2012). Fiji: An open-source platform for biological-image analysis. Nat. Methods *9*, 676–682. https://doi.org/10.1038/nmeth.2019.

83. Wojdyr, M. (2010). Fityk: A general-purpose peak fitting program. J. Appl. Crystallogr. *43*, 1126–1128. https://doi.org/10.1107/S0021889810030499.

84. Villinger, C., Gregorius, H., Kranz, C., Höhn, K., Münzberg, C., Von Wichert, G., Mizaikoff, B., Wanner, G., and Walther, P. (2012). FIB/SEM tomography with TEM-like resolution for 3D imaging of high-pressure frozen cells. Histochem. Cell Biol. *138*, 549–556. https://doi.org/10.1007/s00418-012-1020-6.

85. Edgar, R.C. (2004). MUSCLE: multiple sequence alignment with high accuracy and high throughput. Nucl. Acids Res. *32*, 1792–1797. https://doi.org/10.1093/nar/gkh340.

86. Pinheiro, J., Bates, D., and Core Team, R. (2023). nlme: linear and nonlinear mixed effects models. R package version 3.1-162.

87. Hothorn, T., Bretz, F., and Westfall, P. (2008). Simultaneous inference in general parametric models. Biom. J. *50*, 346–363. https://doi.org/10.1002/bimj.200810425.

88. Felsenstein, J. (1985). Phylogenies and the comparative method. Am. Nat. *125*, 1–15. https://doi.org/10.1086/284325.

89. Pagel, M. (1999). Inferring the historical patterns of biological evolution. Nature *401*, 877–884. https://doi.org/10.1038/44766.

90. Paradis, E., and Schliep, K. (2019). Ape 5.0: An environment for modern phylogenetics and evolutionary analyses in R. Bioinformatics *35*, 526–528. https://doi.org/10.1093/bioinformatics/bty633.

91. Rambaut, A. (2010). Institute of Evolutionary Biology, University of Edinburgh, Edinburgh

STAR★METHODS

KEY RESOURCES TABLE

REAGENT or RESOURCE	SOURCE	IDENTIFIER
Deposited data		
Deposit new data	Dryad	https://datadryad.org/share/Up0r8AmL-aeoeXaP6POl6uRGfODHdl_68cz0d4LkWDg
Bicyclus anynana selected lines	Antónia Monteiro lab	–
Software and algorithms		
pavo v. 2.9 (R package)	Maia et al.[78]	https://doi.org/10.32614/CRAN.package.pavo
Fityk	Wojdyr[79]	https://fityk.nieto.pl/
MUSCLE	Edgar[80]	https://www.drive5.com/muscle/
PhyML	–	http://www.atgc-montpellier.fr/phyml/
R Studio	R core team[81]	https://www.rstudio.com; www.r-project.org/
Fiji	Schindelin et al.[82]	https://imagej.net/software/fiji/
FigTree 1.4.4	Guindon et al.[83]	https://tree.bio.ed.ac.uk/software/figtree/

EXPERIMENTAL MODEL AND STUDY PARTICIPANT DETAILS

Butterfly wing scale sampling

Bicyclus anynana violet-blue lines were previously generated in our laboratory by artificial selection.[15] Scales from other butterfly species were sampled on specimens predominantly from the entomological collection of ETH Zürich (ETHZ), the Lee Kong Chian Natural History Museum (LKCNHM) in Singapore, the Museum National d'Histoire Naturelle (MNHN) in Paris, or alternatively from private insect retailers. Details on specimens and sampled scales are provided in Table S1.

METHOD DETAILS

Scanning electron microscopy (SEM)

Scales were mounted on carbon tape, and sputter coated with platinum for 100 s at 40 mA using a JFC-1600 Fine Coat Ion Sputter (JEOL Ltd, Japan). Samples were imaged using a FEI Versa 3D with the following parameters: voltage 10 kV, current 23 pA. Distances between features in scale images were measured using the Line tool implemented in Fiji.[82] The thickness of the platinum, which differed significantly from the scale in terms of contrast, was excluded in our measurements. For the ridge-ridge distance, 20 measurements were taken per scale with five scales sampled for each genotype. For the crossrib-crossrib distance, 50 measurements were taken per scale with five scales sampled for each genotype. For the window area, 50 measurements were taken per scale with five scales sampled for each genotype.

Focused ion beam scanning electron microscopy (FIB-SEM)

Regular milling

Scales were mounted on carbon tape on which grooves were manually made by drawing lines with a needle. Scales were mounted perpendicularly on top of a groove, having therefore their middle part (where the milling was performed) not directly in contact with the tape but rather in contact with air. Samples were then sputter coated with platinum for 30 s at 30 mA using a JFC-1600 Fine Coat Ion Sputter (JEOL Ltd, Japan). Cross sections of wing scales were obtained by FIB milling using the gallium ion beam of the FEI Versa 3D with the following parameters: beam voltage 8 kV, beam current 12 pA, tilt 52°. Milled samples were imaged using a FEI Versa 3D with the following parameters: voltage 10 kV, current 23 pA. The ridge, crossrib, and air gap thicknesses were measured using the Line tool implemented in Fiji,[82] and corrected for tilted perspective (measured thickness / sin (52°)).[84] Ten independent measurements were taken and averaged.

Ridge milling and post-milling microspectrophotometry

To test the role of ridge height in blue color generation in *M. didius*, we performed a series of FIB-SEM millings followed by reflectance measurement. In this case, scales were mounted on grooved carbon tape without being sputter coated, milled, then the reflectance of the milled samples were measured by microspectrophotometry. To minimize degradation of our uncoated sample by accelerated electrons, we worked at low accelerating voltage (1kV) and low magnification level, and only used snapshots to visualize our sample before milling. To minimize gallium exposure on the area of interest, a region of the scale distant from the targeted milled area was used for Ga beam focusing. Under the usage settings (beam voltage 8 kV, beam current 12 pA), the

duration of the milling depended on the depth: 8s (z = 100 nm), 23s (z = 800 nm), 38s (z = 500 nm), 62s (z = 800 nm), 77s (z = 1000 nm), and 100s (z = 1300 nm). Because the milled regions of interest were tiny ($\leq$ 1 μm^2), we used existing landmarks at a known distance from the region of interest to identify sections with the optical microscope connected to the microspectrophotometer. Once measured, the samples were sputter coated with platinum for 30 s at 30 mA for SEM imaging.

Microspectrophotometry

Scales were individually mounted on grooved carbon tape. Reflectance spectra, with a usable range of 340-950 nm, were acquired under normal incidence with a microspectrophotometry set-up including a mercury-xenon light source (Thorlabs, New Jersey, USA) connected to a uSight-2000-Ni microspectrophotometer (Technospex Pte. Ltd, Singapore), using a polished aluminium mirror as a light reference. The microscope's Nikon TU Plan Fluor objectives have the following specifications: 20x (NA = 0.5), 100x (NA = 0.9). The spot size of the microspectrophotometer is between 1.1 and 1.2 μm when coupled with the 100x objective. Each measurement was averaged 10 times over an integration time of 100 ms. Reflectance spectra were obtained by averaging three measurements taken at different locations on the scale to account for variability. Reflectance spectra were analysed, smoothed with span = 0.2, and plotted using the R package pavo version 2.9.[78]

Upper and lower scale surfaces dissociation

In *B. anynana*, measurements of reflectance were performed on the upper surface, *i.e.* ridges and crossribs, separated from the lower lamina. An individual ground scale was collected from wings using a fine needle, mounted on a glass slide, then immobilized by placing a cover slip over one third of its surface area while maintaining a soft pressure with one hand. The exposed two thirds of the scale were softly brushed with a paintbrush to create micro breaking points. With the other hand, a piece of double-sided tape was applied on a small fraction of the scale until a fragment of the upper surface adhered to it and was hanging free from the edge of the tape. This "free hanging" scale area was used for measuring the color of the ridges and crossribs by microspectrophotometry.

Scale depigmentation

Scales were collected from wings using a fine needle, then individually mounted on a glass slide. A drop of sodium hypochlorite (bleach) 5.25% was applied on the scale with a micropipette. After one minute in bleach, the scale was rinsed twice in milliQ® ultrapure water, then allowed to dry on the glass slide at room temperature prior to reflectance measurements. Pigments are known to reduce light back scattering, and thus prevent the generated structural color from being washed away. After pigmentation removal, reflectance values were lower than in untreated scales. To buffer this effect, we placed a piece of carbon tape under the glass slide, right below the scale sample, before measuring the reflectance (Figure S5).

Optical simulation

The electromagnetic simulations were conducted using a two-dimensional finite-difference time-domain (FDTD) method. A complex refractive index was used for chitin with the refractive index (real part) n = 1.56 and the extinction coefficient (imaginary part) k = 0.06.[40] A broadband plane wave was normally incident to periodic arrays of either full ridges, ridges with partially milled core and lamellae, or ridges with partially milled lamellae. The perfectly matched layer-absorbing boundary condition was applied along the light propagation direction to absorb light outside the structure regions. Energy monitors were placed behind the light source to record the reflected light. Input values of the model are indicated in Figure S8. Detailed discussion for the newly described interference model used in Figure 4D is available in.[39]

Phylogenetic reconstruction

Sequences were retrieved from a previously published phylogenomic analysis of butterflies that includes 352 loci from 207 species representing 98% of the tribes.[26] If this dataset did not include the same species used in our study, we selected the closest species or tribe available (see Table S2). After selection of relevant taxa, nucleotide sequences were re-aligned with MUSCLE.[85] Maximum-likelihood searches were performed using PhyML 3.0[79] under the GTR matrix with optimization of site substitution rates and final likelihood evaluation using a gamma distribution. One-thousand bootstrap replicates were conducted for support estimation.

QUANTIFICATION AND STATISTICAL ANALYSIS

Color quantification

Raw spectral data were imported into R and processed with the package pavo version 2.9.[78] Negative values were converted to zero, spectra were averaged across samples, and curves were smoothed (span = 0.2). The reflectance spectra were analyzed to estimate parameters such as wavelength, intensity, and saturation of the reflectance peak. The full-width at half-maximum (FWHM) of the reflectance peak characterizes the desaturation, opposite of saturation.[80] These parameters were calculated using the peakshape() function of the R package pavo. The FWHM was calculated using the absolute minimum reflectance of the spectrum. When the R package pavo failed to identify optical peak parameters, we used a split Gaussian function with a Levenberg-Marquardt least square method to fit all the spectral features, using the open-source program Fityk.[83]

Statistical analysis

The differences in mean height/thickness, distance, or window area between the *B. anynana* wildtype and blue lines were analyzed using a linear mixed model (LME) that allows both fixed and random effects. The rationale was the non-independent, hierarchical nature of the data with multiple measurements taken from each scale, and multiple scales for each individual. The scale type (wild type WT, generation G6, generation G8) was treated as the fixed factor, and the scale nested within individual as a random factor. LME was run using the nlme 3.1 package,[86] and different models were compared using the Akaike information criterion (AIC) method. The lack of homogeneity of variances among scale types prompted us to use the varIdent() function in the nmle package. Adjusted *P*-values for different pairwise comparisons were obtained by the Bonferroni post hoc analysis using the multcomp 1.4 package[87] and Tukey contrasts. Outputs of the LME tests and adjusted *P*-values for multiple comparisons are shown in Tables S3 and S4.

For correlation studies, we used the phylogenetic generalized least squares (PGLS) method that incorporates phylogenetic relatedness to account for non-independence of data points between the species in our sample.[88] We used the gls function with Pagel's lamba correlation structure[89] from the nlme 3.1[86] and ape 5.0[90] R packages. Newick tree files were converted into Nexus tree files using the software FigTree 1.4.4.[91] Statistical analysis and plots were done with R 4.2.2.[81]